Neurobiology of Disease

Early-Onset Epileptic Encephalopathy Caused by Gain-of-Function Mutations in the Voltage Sensor of $K_v7.2$ and $K_v7.3$ Potassium Channel Subunits

Francesco Miceli,[1]* Maria Virginia Soldovieri,[2]* Paolo Ambrosino,[2] Michela De Maria,[2] Michele Migliore,[3] Rosanna Migliore,[3] and Maurizio Taglialatela[1,2]

[1]Department of Neuroscience, University of Naples Federico II, 80131 Naples, Italy, [2]Department of Medicine and Health Science, University of Molise, 86100 Campobasso, Italy, and [3]Institute of Biophysics, National Research Council, 90146 Palermo, Italy

Mutations in *$K_v7.2$* (*KCNQ2*) and *$K_v7.3$* (*KCNQ3*) genes, encoding for voltage-gated K^+ channel subunits underlying the neuronal M-current, have been associated with a wide spectrum of early-onset epileptic disorders ranging from benign familial neonatal seizures to severe epileptic encephalopathies. The aim of the present work has been to investigate the molecular mechanisms of channel dysfunction caused by voltage-sensing domain mutations in $K_v7.2$ (R144Q, R201C, and R201H) or $K_v7.3$ (R230C) recently found in patients with epileptic encephalopathies and/or intellectual disability. Electrophysiological studies in mammalian cells transfected with human $K_v7.2$ and/or $K_v7.3$ cDNAs revealed that each of these four mutations stabilized the activated state of the channel, thereby producing gain-of-function effects, which are opposite to the loss-of-function effects produced by previously found mutations. Multistate structural modeling revealed that the R201 residue in $K_v7.2$, corresponding to R230 in $K_v7.3$, stabilized the resting and nearby voltage-sensing domain states by forming an intricate network of electrostatic interactions with neighboring negatively charged residues, a result also confirmed by disulfide trapping experiments. Using a realistic model of a feedforward inhibitory microcircuit in the hippocampal CA1 region, an increased excitability of pyramidal neurons was found upon incorporation of the experimentally defined parameters for mutant M-current, suggesting that changes in network interactions rather than in intrinsic cell properties may be responsible for the neuronal hyperexcitability by these gain-of-function mutations. Together, the present results suggest that gain-of-function mutations in $K_v7.2/3$ currents may cause human epilepsy with a severe clinical course, thus revealing a previously unexplored level of complexity in disease pathogenetic mechanisms.

Key words: **epileptic encephalopathies; gating; K_v7 potassium channels; mutations; voltage-sensing domain**

Introduction

Epileptic encephalopathies (EEs) are clinical conditions in which epileptiform abnormalities contribute to progressive disturbance in cerebral function; three main features characterize EEs: epileptic seizures (often poorly responsive to pharmacological treatment), EEG abnormalities, and various degrees of developmental delay. Genetic research in the past two decades has identified several EE genes and provided novel hints into disease pathogenesis (Cross and Guerrini, 2013); however, how mutations in specific genes contribute to the severity of the epilepsy phenotype is largely unknown (Striano et al., 2013).

Mutations in *$K_v7.2$* (*KCNQ2*) and *$K_v7.3$* (*KCNQ3*) genes, encoding for voltage-gated K^+ channel subunits underlying the neuronal M-current (I_{KM}) (Wang et al., 1998), are responsible for early-onset epileptic diseases with a widely diverging phenotypic presentation. Earlier studies revealed that *$K_v7.2$* (Biervert et al., 1998; Singh et al., 1998) or, more rarely, *$K_v7.3$* (Charlier et al., 1998) gene defects are responsible for benign familial neonatal seizures (BFNSs), an autosomal-dominant epilepsy of newborns. BFNS-affected patients suffer from recurrent seizures that begin in the very first days of life and remit after a few weeks or months, with mostly normal interictal EEG, neuroimaging, and psychomotor development. Following several reports questioning the benignity of the clinical course in BFNS patients (Steinlein et al., 2007), *de novo* missense $K_v7.2$ mutations have been more recently found in neonates affected with pharmacoresistant seizures, distinct EEG and neuroradiological features, and various degrees of developmental delay, defining a "$K_v7.2$ encephalopa-

Received Oct. 24, 2014; revised Dec. 30, 2014; accepted Jan. 19, 2015.

Author contributions: M.M. and M.T. designed research; F.M., M.V.S., P.A., M.D.M., R.M., and M.M. performed research; F.M., M.V.S., P.A., M.D.M., R.M., M.M., and M.T. analyzed data; M.M. and M.T. wrote the paper.

This work was supported by Telethon Grant GGP07125, the Fondazione San Paolo-IMI (Project Neuroscience), Regione Molise (Convenzione AIFA/Regione Molise), the Science and Technology Council of the Province of Avellino, Grant PRIN 2009 to M.T., and the Fondazione Umberto Veronesi to F.M. We thank Dr. Thomas J. Jentsch, Department of Physiology and Pathology of Ion Transport, Leibniz-Institut für Molekulare Pharmakologie, Berlin for sharing Kv7.2 and Kv7.3 cDNAs; Dr. Alvaro Villarroel, Unidad de Biofisica, UPV-CSIC, Leioa, Spain for sharing Kv7.3 A315T cDNA; Dr. David E. Shaw, D.E. Shaw Research, New York, for the coordinates of the Kv1.2/2.1 chimera. F.M. and M.V.S. are supported by postdoctoral fellowships from the Department of Neuroscience, University of Naples Federico II, Naples, and from the Italian Society for Pharmacology, respectively.

The authors declare no competing financial interests.

*F.M. and M.V.S. contributed equally to this work.

Correspondence should be addressed to Dr. Maurizio Taglialatela, Department of Medicine and Health Sciences, University of Molise, Via De Sanctis, 86100 Campobasso, Italy. E-mail: m.taglialatela@unimol.it.

DOI:10.1523/JNEUROSCI.4423-14.2015

Copyright © 2015 the authors 0270-6474/15/353782-12$15.00/0

thy" (Weckhuysen et al., 2012). Subsequently, *de novo* missense $K_v7.2$ mutations have been also shown as one of the most common causes of early-onset EEs, including the Ohtahara syndrome (Saitsu et al., 2012; Kato et al., 2013), the most severe and earliest developing age-related EE.

Functional studies have revealed that BFNS-causing mutations decrease I_{KM} conductance, and a 25% reduction in $K_v7.2/3$ currents appears sufficient to increase neuronal excitability to epileptogenic levels in early infancy (Jentsch, 2000); animal models appear to confirm such conclusion (Singh et al., 2008). More dramatic functional deficits have been found in channels carrying mutations associated with more severe epileptic phenotypes (Miceli et al., 2013; Orhan et al., 2014).

In the present work, mutagenesis, electrophysiology, biochemical, multistate modeling, and computational modeling techniques have been used to investigate the molecular mechanisms underlying disease pathogenesis by three voltage-sensing domain (VSD) mutations in $K_v7.2$ (R144Q, Allen et al., 2013; R201C, Weckhuysen et al., 2013; and R201H, Carvill et al., 2013) or $K_v7.3$ (R230C, Rauch et al., 2012; Allen et al., 2013) recently described in patients with EE and/or intellectual disability. Together, the results obtained reveal that all four these mutations stabilize the activated state configuration of the VSD, suggesting that, in addition to a loss-of-function (LOF), a gain-of-function (GOF) mechanism in $K_v7.2/3$ currents may also cause human epilepsy with a severe clinical course.

Materials and Methods

Mutagenesis and heterologous expression of $K_v7.2$ and $K_v7.3$ cDNAs. Mutations were engineered in human $K_v7.2$ or $K_v7.3$ cDNAs cloned into pcDNA3.1 by QuickChange site-directed mutagenesis (Agilent Technologies), as previously described (Miceli et al., 2013). Channel subunits were expressed in Chinese Hamster Ovary (CHO) cells from female animals by transient transfection. CHO cells were grown in 100 mm plastic Petri dishes in DMEM containing 10% FBS, penicillin (50 U/ml), and streptomycin (50 μg/ml) in a humidified atmosphere at 37°C with 5% CO_2. For electrophysiological experiments, cells were seeded on glass coverslips (Carolina Biological Supply) in 40-mm dishes and transfected on the next day with the appropriate cDNAs using Lipofectamine 2000 (Invitrogen) according to the manufacturer's protocol. A plasmid encoding for enhanced green fluorescent protein (Clontech) was used as transfection marker; total cDNA in the transfection mixture was kept constant at 4 μg. For biotinylation experiments, cells were seeded on 60-mm dishes and transfected with 6 μg of total cDNA.

Whole-cell electrophysiology. Currents from CHO cells were recorded at room temperature (20°C–22°C) 1–2 d after transfection, using a commercially available amplifier (Axopatch 200B, Molecular Devices) and the whole-cell configuration of the patch-clamp technique, with glass micropipettes of 3–5 MΩ resistance. The extracellular solution contained (in mM) the following: 138 NaCl, 5.4 KCl, 2 $CaCl_2$, 1 $MgCl_2$, 10 glucose, and 10 HEPES, pH 7.4 with NaOH; when higher (50 mM) KCl concentrations were used, the NaCl concentration was decreased accordingly. The pipette (intracellular) solution contained (in mM) the following: 140 KCl, 2 $MgCl_2$, 10 EGTA, 10 HEPES, 5 Mg-ATP, pH 7.3–7.4 with KOH. The pCLAMP software (version 10.0.2) was used for data acquisition and analysis. Linear cell capacitance (C) and series-resistance (R_S) calculation, were performed as described previously (Soldovieri et al., 2007). All illustrated and analyzed currents were corrected offline for linear capacitance and leakage currents using standard subtraction routines (Clampfit module of pClamp 10). Current densities (expressed in picoamperes per picofarad) were calculated as peak K^+ currents at 0 mV divided by C. Data were acquired at 0.5–2 kHz and filtered at 1–5 kHz with the 4-pole low-pass Bessel filter of the amplifier. No corrections were made for liquid junction potentials. To generate conductance-voltage curves, the cells were held at −80 mV, then depolarized for 1.5 s from −80 mV to 20/80 mV in 10 mV increments, followed by an isopotential pulse at 0 mV of 300 ms duration; the current values recorded at the beginning of the 0 mV pulse were measured, normalized, and expressed as a function of the preceding voltages. The data were then fit to a Boltzmann distribution of the following form: $y = max/[1 + exp(V_{1/2} - V)/k]$, where V is the test potential, $V_{1/2}$ the half-activation potential, and k the slope factor. Activation current traces were fit to a double-exponential function; a single time constant representing the weighted average of the slow and fast components was obtained by using the following equation: $\tau = (\tau_f A_f + \tau_s A_s)/(A_f + A_s)$, where A_f and A_s indicate the amplitude of the fast and slow exponential components, respectively, and τ_f and τ_s indicate the time constants of these components. Resting membrane potential in CHO cells was determined in current clamp after achieving the whole-cell configuration; recordings were sampled at 10 kHz and filtered at 5 kHz via a 4-pole Bessel low-pass filter.

Cell surface biotinylation and Western blotting. Plasma membrane expression of wild-type and mutant $K_v7.2$ or $K_v7.3$ subunits in CHO cells was investigated by surface biotinylation of membrane proteins in transfected cells 1 d after transfection using Sulfo-NHS-LC-Biotin (Pierce), a cell-membrane impermeable reagent, as previously described (Borgatti et al., 2004; Castaldo et al., 2004). Following cell transfection, biotinylation, and lysis, a fraction of cell lysates were reacted with ImmunoPure immobilized streptavidin beads (Pierce). Channel subunits in streptavidin precipitates and total lysates were analyzed by Western blotting on 8% SDS-PAGE gels using mouse monoclonal anti-$K_v7.2$ (clone N26A/23, dilution 1:1000; Antibodies Inc.) or rabbit polyclonal anti-$K_v7.3$ (clone APC-051, dilution 1:1000; Alomone Labs) antibodies, followed by HRP-conjugated anti-mouse or anti-rabbit secondary antibodies (clone NA931V or NA934V, respectively; dilution 1:5000; GE Healthcare). Reactive bands were detected by chemiluminescence (ECL Western Blotting Substrate; Promega). To confirm that the biotinylation reagent did not leak into the cell and label intracellular proteins and to check for equal protein loading, the same blots were also probed with anti-α-tubulin antibodies (dilution 1:2000; Sigma). Acquisition and data analysis were performed by using ImageLab software (version 4.1; Bio-Rad).

Computational modeling. To study the possible mechanisms through which an increase in $K_v7.2/3$-I_{KM} function can enhance neuronal excitability, we used a realistic model of a hippocampal pyramidal CA1 neuron taken from a previous work (cell 5038804 from Migliore et al., 2005) (ModelDB a.n. 55035), and whose active and passive properties have already been validated against several experimental findings (e.g., Migliore, 2003; Marcelin et al., 2009; Ascoli et al., 2010). For one set of simulations, we included an interneuron, connected in such a way to implement a feedforward inhibitory microcircuit in which the effects of an excitatory Schaeffer collateral input is modulated by perisomatic inhibition. The model files for the interneuron were taken from a previous work (model DB a.n. 87546) performed to support and explain experimental findings (Minneci et al., 2007). The resting potential was set for both neurons at −65 mV. Biophysical properties of wild-type and mutant $K_v7.2/3$ currents were implemented according to the experimental findings (Table 1; $K_v7.2+K_v7.3$ and $K_v7.2+K_v7.2$R201C$+K_v7.3$ for wild-type and mutant, respectively). In both cells, I_{KM} was inserted into the soma at the same density, whereas it was threefold higher in the axon of the CA1 pyramidal neuron (Shah et al., 2008). I_{KM} peak conductance at the soma was determined in such a way to be consistent with the peak I_{KM} current measured from whole-cell somatic voltage-clamp experiments (for the hippocampal interneuron and principal cell, respectively: Hu et al., 2002; Lawrence et al., 2006). With our CA1 pyramidal and interneuron model morphologies, and the I_{KM} kinetics implemented with the experimental data obtained, a value of 15 pS/μm^2 for both the CA1 and the interneuron resulted in the experimentally observed 1 nA peak value during a simulation of a whole-cell somatic voltage-clamp to 40 mV (from −60 mV) for the interneuron (Lawrence et al., 2006), and 0.6 nA for a voltage-clamp at −20 mV for the CA1 principal cell (Hu et al., 2002, 2007). Under control conditions (i.e., wild-type I_{KM} with a 15 pS/μm^2 peak conductance), the interneuron had an input resistance much higher than the principal cell (260 vs 60 MΩ), in agreement with experimental findings (Foster and Dumas, 2001; Lamsa et al., 2007; Zemankovics et al., 2010). To model the synchronous activation of an afferent Schaeffer collateral volley, a single suprathreshold (39 nS)

Table 1. Biophysical and pharmacological properties of mutant $K_v7.2$ and $K_v7.3$ channels

	n	$V_{½}$ (mV)	k (mV/efold)	$I_{instant}/I_{steady\text{-}state}$	Current density (pA/pF)	Resting membrane potential (mV) (in 5.4 or 50 mM K^+)	Blockade by TEA (%)		
							0.3 mM	3 mM	30 mM
Nontransfected CHO cells	10	—	—	—	0.5 ± 0.1	−15.0 ± 2.8 (5.4); −10.5 ± 2.2 (50)	—	—	—
$K_v7.2$	23	−26.7 ± 1.1	12.6 ± 0.5	0.04 ± 0.02	31 ± 3	—	59.0 ± 3.1	86.7 ± 2.3	93.3 ± 6.0
$K_v7.2$ R144Q	11	−46.9 ± 1.8*	18.2 ± 1.0*	0.17 ± 0.03	37 ± 7	—	—	90.7 ± 5.2	—
$K_v7.2$ R201C	12	—	—	0.86 ± 0.04	60 ± 6*	—	60.3 ± 3.0	91.8 ± 2.1	96.9 ± 1.6
$K_v7.2$ R201H	7	−56.1 ± 4.1*	25.7 ± 0.9*	0.46 ± 0.07	51 ± 6*	—	—	91.5 ± 2.9	—
$K_v7.3$	18	−38.2 ± 1.1	7.2 ± 0.4	0.04 ± 0.02	10 ± 1	—	—	—	64.3 ± 1.9
$K_v7.3$ R230C	13	—	—	1.00 ± 0.01	121 ± 21**	—	—	—	54.7 ± 9.6
$K_v7.2 + K_v7.2$ R144Q	7	−37.7 ± 2.0*	15.3 ± 0.4	—	34 ± 5	—	—	—	—
$K_v7.2 + K_v7.2$ R201C	7	−47.9 ± 3.0*	19.2 ± 3.3*	—	41 ± 7	—	—	—	—
$K_v7.2 + K_v7.2$ R201H	9	−41.2 ± 1.3	15.0 ± 0.7	—	40 ± 6	—	—	—	—
$K_v7.2 + K_v7.3$	17	−33.0 ± 1.1	12.1 ± 0.9	0.04 ± 0.02	114 ± 7	−51.0 ± 1.1 (5.4); −23.1 ± 1.5 (50)	16.3 ± 3.5	49.0 ± 4.3	77.5 ± 4.0
$K_v7.2$ R144Q + $K_v7.3$	9	−42.8 ± 2.7†	11.8 ± 0.4	0.03 ± 0.02	113 ± 23	−52.0 ± 1.1 (5.4)	—	—	—
$K_v7.2$ R201C + $K_v7.3$	7	−60.8 ± 2.3†	16.8 ± 2.3†	0.37 ± 0.04	132 ± 10	−69.2 ± 2.3 (5.4)†; −23.7 ± 1.2 (50)	—	—	—
$K_v7.2$ R201H + $K_v7.3$	6	−45.4 ± 1.8†	17.3 ± 0.7†	0.16 ± 0.02	131 ± 26	−69.2 ± 2.2 (5.4)†	—	—	—
$K_v7.2 + K_v7.3$ R230C	8	−42.6 ± 3.1†	15.9 ± 1.2†	0.11 ± 0.05	83 ± 8	−62.3 ± 2.7 (5.4)†	—	—	—
$K_v7.2 + K_v7.2$ R144Q + $K_v7.3$	7	−33.8 ± 2.9	11.3 ± 0.7	0.03 ± 0.01	118 ± 53	−57.0 ± 6.7 (5.4); −21.7 ± 2.1 (50)	19.0 ± 10.4	49 ± 12	88.2 ± 3.0
$K_v7.2 + K_v7.2$ 201C + $K_v7.3$	7	−42.4 ± 2.5†	13.3 ± 0.8	0.11 ± 0.02	136 ± 12	−62.4 ± 1.0 (5.4)†; −24.6 ± 0.4 (50)	14.0 ± 4.5	52.1 ± 7.0	88.4 ± 1.8
$K_v7.2 + K_v7.2$ R201H + $K_v7.3$	9	−39.9 ± 1.9†	13.2 ± 0.8	0.07 ± 0.02	100 ± 23	−64.1 ± 1.6 (5.4)†; −22.3 ± 2.0 (50)	9.9 ± 1.1	43.6 ± 6.0	79.0 ± 4.2
$K_v7.2 + K_v7.3$ R230C + $K_v7.3$	7	−39.9 ± 3.7†	15.3 ± 0.7	0.10 ± 0.03	86 ± 6	−62.0 ± 2.4 (5.4)†; −21.8 ± 0.5 (50)	14.0 ± 6.2	47.1 ± 10	77.0 ± 7.3

*$p < 0.05$ versus $K_v7.2$; **$p < 0.05$ versus $K_v7.3$; †$p < 0.05$ versus $K_v7.2 + K_v7.3$.

excitatory synaptic conductance was randomly activated (Poisson) at an average frequency of 50 Hz (in the range of the gamma rhythm), on the main apical trunk at 100 μm from the soma. Its kinetics was implemented with a double exponential conductance change (0.5 and 5 ms for rise and decay time constant), and a reversal potential of 0 mV. For the simulations of a microcircuit, the same excitatory input (22 nS) was relayed to the soma of the interneuron with a 3 ms delay. The action potentials of the interneuron were then used to activate an inhibitory synapse (0.5 and 7 ms for rise and decay time constant and a reversal potential of −80 mV) on the soma of the principal cell.

Simulations were performed using the NEURON simulation environment (version 7.3; Hines and Carnevale, 1997). Model and simulation files will be available for public download on the ModelDB section of the Senselab suite (http://senselab.med.yale.edu).

Multistate structural modeling. Three-dimensional models of $K_v7.2$ subunits were generated by using as templates the coordinates of six different states of $K_v1.2/2.1$ paddle chimera (PDB accession number 2R9R; 29% of sequence identity with $K_v7.2$) obtained in molecular dynamics simulations (Jensen et al., 2012). Modeling of the S1-S4 VSD in each state was performed with SWISS-MODEL, as described previously (Miceli et al., 2013). The models were optimized through all-atom energy minimization by using the GROMOS96 implementation of Swiss-PDBViewer and analyzed using both the DeepView module of Swiss-PDBViewer (version 4.0.1; http://spdbv.vital-it.ch/) and PyMOL (http://www.pymol.org/).

Statistics. Data are expressed as the mean ± SEM. Statistically significant differences between the data were evaluated with the Student's *t* test ($p < 0.05$).

Results

Gating changes in homomeric $K_v7.2$ channels carrying the R144Q, R201C, or R201H mutations

The schematic topology of a single K_v7 subunit and the location of the mutations investigated are shown in Figure 1*A*. Three of the four mutations affect the second positively charged residue (R2) along the S4 sequence in the VSD of $K_v7.2$ (R201C, Weckhuysen et al., 2013; and R201H, Carvill et al., 2013) or $K_v7.3$ (R230C, Rauch et al., 2012; Allen et al., 2013); the fourth, instead, neutralizes the R at the bottom of S2 in $K_v7.2$ (R144Q, Allen et al., 2013). Both these residues are highly conserved among K_v channels (Fig. 1*B*).

In transiently transfected CHO cells, homomeric $K_v7.2$ channels generated time-dependent, K^+-selective currents that slowly activate at a threshold potential ~−50 mV (Fig. 2*A*). At the holding voltage of −80 mV, the vast majority of $K_v7.2$ channels were closed; therefore, the ratio between the currents measured at the beginning of the depolarization step ($I_{Instant}$) and those at the end of the 0 mV depolarization ($I_{steady\text{-}state}$) was close to 0 (Table 1). By contrast, at −80 mV, homomeric $K_v7.2$ R201C channels showed an almost complete loss of time dependence in current activation kinetics (Fig. 2*A*); therefore, the $I_{Instant}/I_{steady\text{-}state}$ ratio was greatly increased (Table 1). Although the G/V curve of $K_v7.2$ channels was sigmoidal, $K_v7.2$ R201C currents showed a mostly linear G/V between 20 mV and −80 mV, indicative of a significant loss of voltage-dependent gating (Fig. 2*B*); a slight degree of channel deactivation could be observed upon membrane hyperpolarization below the holding voltage. In $K_v7.2$, the replacement of the same R2 residue with an H (R201H) caused a marked hyperpolarizing shift (~30 mV) in the voltage dependence of current activation (Fig. 2*A*,*B*; Table 1). A significant fraction of $K_v7.2$ R201H channels was open at −80 mV (Table 1). Qualitatively similar but less dramatic functional changes were observed in homomeric $K_v7.2$ R144Q mutant channels, whose G/V curve was shifted by 20 mV to more negative potentials (Fig. 2*A*,*B*; Table 1). Despite such dramatic changes in voltage-dependent gating, all mutant channels retained their K^+ selectivity; indeed, the reversal potential of the currents from $K_v7.2$ (−79 ± 1 mV), $K_v7.2$ R201C (−79 ± 1 mV), $K_v7.2$ R201H (−76 ± 1 mV), and $K_v7.2$ R144Q (−76 ± 2 mV) channels was close to that of a K^+-selective pore (−83 mV under the present recording conditions). Tetraethylammonium (TEA) sensitivity was also unaffected in all three mutant channels (Table 1), confirming that these mutations do not alter pore structure. K^+ currents recorded in cells expressing $K_v7.2$ channels show double exponential activation kinetics, with the fast component (A_f) accounting for ~90% of the total activation process (Soldovieri et al., 2007). Compared with $K_v7.2$ channels, noninstantaneous currents from $K_v7.2$ R144Q or $K_v7.2$ R201H mutant channels displayed similar kinetics in the voltage range between −50 mV and −10 mV; a significant increase in the weighted average of τ was only ob-

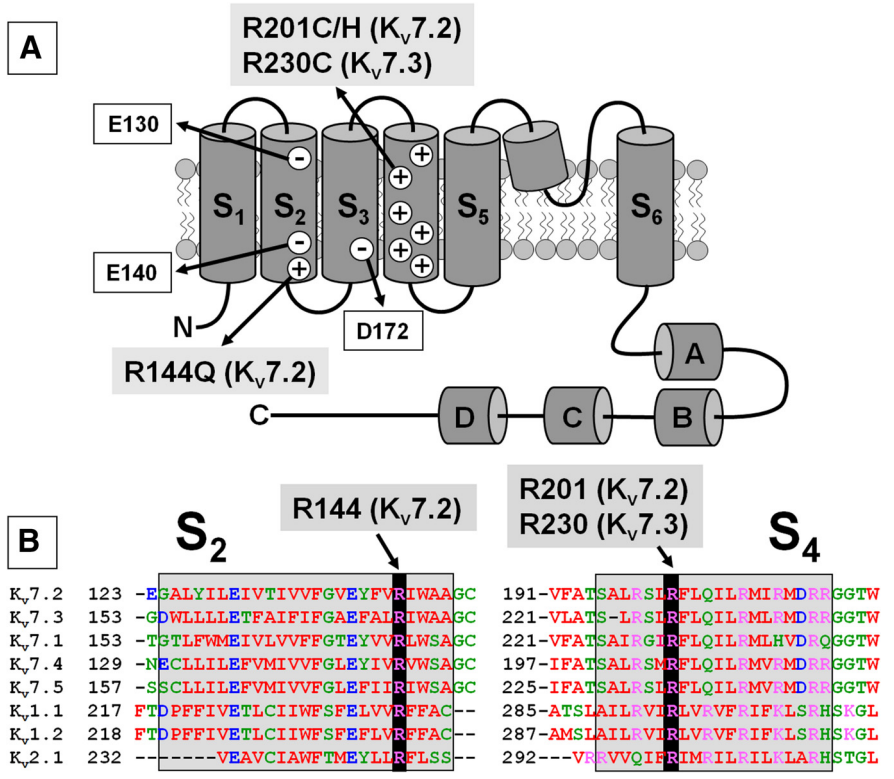

Figure 1. Schematic drawing of a K_v7 subunit and location of the naturally-occurring mutations studied in the present work. ***A***, Topological representation of a single K_v7 subunit. Arrows indicate the location of the mutations investigated (shaded in gray); the negatively charged residues E130 and E140 in S2, and D172 in S3, are boxed in white. A–D indicate the four putative α-helical domains identified in the K_v7 C-terminal region. ***B***, Sequence alignment of the S2 and S4 segments of the indicated K_v subunits (www.ebi.ac.uk/Tools/psa/). Residues are colored according to the following scheme: magenta represents basic; blue represents acid; red represents nonpolar; green represents polar.

served at more positive potentials (from 0 to 20 mV). Indeed, at 0 mV, the weighted average of τ was 103 ± 20, 372 ± 38, and 219 ± 40 ms for $K_v7.2$, $K_v7.2$ R144Q, and $K_v7.2$ R201H, respectively ($n = 6$; $p < 0.05$).

Figure 2*C* shows a superposition of current traces from $K_v7.2$, $K_v7.2$ R144Q, $K_v7.2$ R201C, and $K_v7.2$ R201H channels in response to a subthreshold depolarizing pulse of −60 mV, followed by a stronger depolarization to 0 mV. At −60 mV, no current flowed through $K_v7.2$ channels, whereas significant outward currents could be recorded in cells expressing $K_v7.2$ R144Q, R201H, and R201C mutant channels.

Functional properties of homomeric $K_v7.3$ channels carrying the R230C substitution

Compared with $K_v7.2$, homomeric $K_v7.3$ channels generate currents of smaller size, lower TEA sensitivity, and negatively shifted activation gating (Fig. 3*A*,*B*; Table 1) (Wang et al., 1998; Soldovieri et al., 2006). Neutralization of R2 with a C ($K_v7.3$ R230C) fully eliminated both voltage and time dependence of current gating in the voltage range between −100 and 20 mV (Fig. 3*A*,*B*; Table 1), thus producing functional consequences largely similar to those previously described for the corresponding R201C mutation in $K_v7.2$. The reversal potential (−80 ± 1 mV) and TEA sensitivity (Table 1) of $K_v7.3$ R230C currents were unchanged compared with $K_v7.3$ channels. The K^+ current density recorded in $K_v7.3$ R230C-expressing cells was ~12 times larger than in those expressing $K_v7.3$; a similar, but less dramatic, effect was also observed when the R201C mutation was introduced in $K_v7.2$ (Table 1). The increased current size observed in $K_v7.3$ R230C-transfected cells does not appear to be consequent to a mutation-induced increase in plasma membrane subunit expression. Indeed, Western blot experiments revealed no difference in the ratios between the intensities of the 90 kDa band (corresponding to wild-type or mutant $K_v7.3$ subunits) and the α-tubulin band (~55 kDa) in total lysates from $K_v7.3$- and $K_v7.3$ R230C-transfected cells; the $OD_{Q3\text{-}TOTAL}/OD_{TUB}$ ratios were 1.00 ± 0.16 and 1.15 ± 0.26 for $K_v7.3$ and $K_v7.3$ R230C, respectively ($n = 3$; $p > 0.05$; Fig. 3*C*, top). More importantly, the ratios between the intensities of the Kv7.3 band in streptavidin-isolated plasma membrane proteins and in total lysates from the same cells were also identical, as the $OD_{Q3\text{-}BIOT}/$

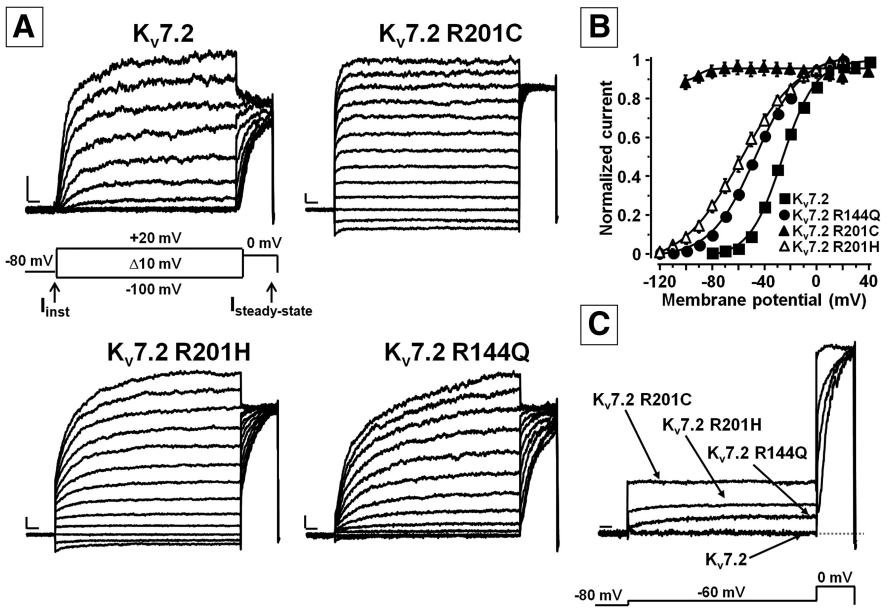

Figure 2. Functional properties of wild-type and mutant homomeric $K_v7.2$ channels. ***A***, Macroscopic currents from $K_v7.2$, $K_v7.2$ R201C, $K_v7.2$ R201H, or $K_v7.2$ R144Q channels, in response to the indicated voltage protocol. The arrows on the voltage protocol indicate the time chosen for current analysis, as explained in the text. Current scale, 100 pA; time scale, 0.1 s. ***B***, Conductance/voltage curves for the indicated channels. Continuous lines are Boltzmann fits to the experimental data. Each data point is the mean ± SEM of 7–20 cells recorded in at least three separate experimental sessions. ***C***, Normalized and superimposed current traces from the indicated channels in response to the voltage protocol shown. Time scale, 0.1 s.

$OD_{Q3\text{-}TOTAL}$ ratios were 2.77 ± 0.58 and 2.00 ± 0.62 for $K_v7.3$ and $K_v7.3$ R230C, respectively ($n = 3$; $p > 0.05$; Fig. 3*C*, bottom). Plasma membrane expression of another $K_v7.3$ mutation (A315T), which also markedly increased macroscopic current size (Zaika et al., 2008), was also unaffected ($OD_{Q3\text{-}TOTAL}/OD_{TUB}$ were 0.75 ± 0.20; $OD_{Q3\text{-}BIOT}/OD_{Q3\text{-}TOTAL}$ were 1.46 ± 0.83; $n = 3$; $p > 0.05$ vs $K_v7.3$) (Fig. 3*C*), confirming that most homomeric $K_v7.3$ channels are functionally silent but may be unlocked into a conductive conformation by specific mutations.

Effect of mutant subunits incorporation into heteromeric channels with $K_v7.2$ and/or $K_v7.3$ subunits

To mimic the genetic condition of the affected patients, who carry a single mutant allele, and considering that I_{KM} is mainly formed by heteromeric assembly of $K_v7.2$ and $K_v7.3$ subunits (Wang et al., 1998), the functional consequences of the described mutations were also assessed in heteromeric channels formed upon coexpression of $K_v7.2$ and/or $K_v7.3$ subunits. To this aim, CHO cells were transfected with $K_v7.2$+$K_v7.3$ cDNAs at a 1:1 ratio (to mimic the genetic balance of normal individuals), $K_v7.2$+$K_v7.2$ R201C+$K_v7.3$, $K_v7.2$+$K_v7.2$ R201H+$K_v7.3$, and $K_v7.2$+$K_v7.2$ R144Q+$K_v7.3$ at 0.5:0.5:1 ratio (to mimic the genetic balance of heterozygous individuals who carried mutant Kv7.2 alleles), or $K_v7.2$+ $K_v7.3$+ $K_v7.3$ R230C at 1:0.5:0.5 ratio (to mimic the genetic balance of the heterozygous individual carrying the mutant $K_v7.3$ allele).

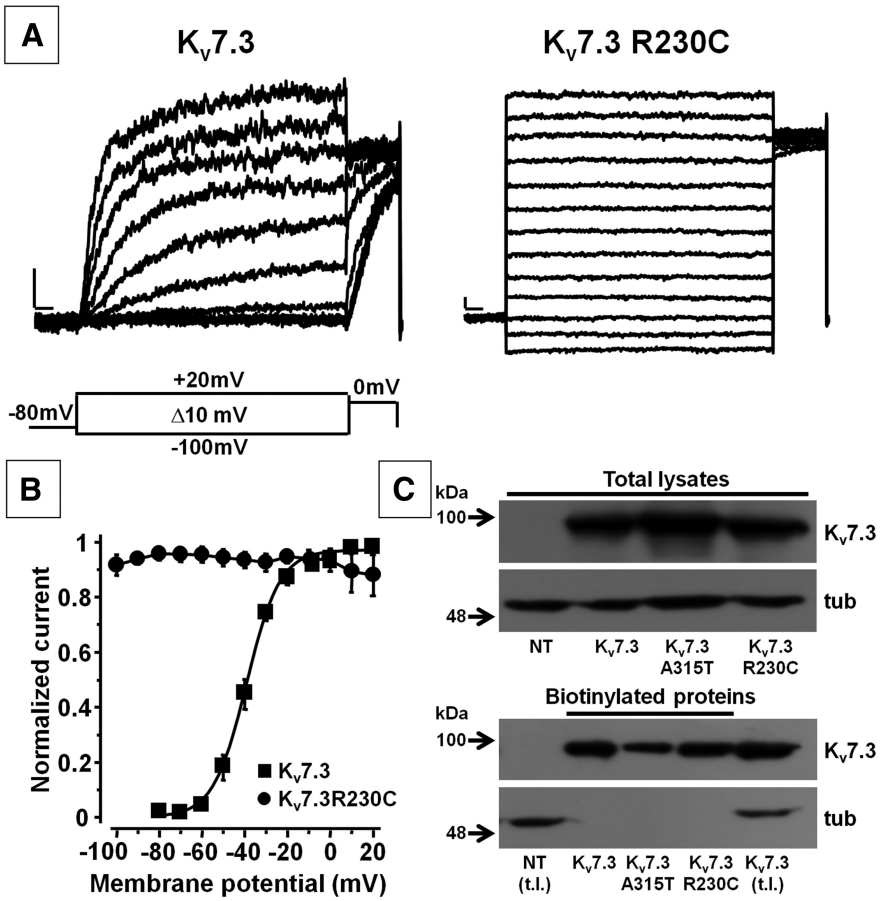

Figure 3. Functional properties of homomeric $K_v7.3$ and $K_v7.3$ R230C channels. ***A***, Macroscopic currents from $K_v7.3$ and $K_v7.3$ R230C channels, in response to the indicated voltage protocol. Current scale, 50 pA; time scale, 0.1 s. ***B***, Conductance/voltage curves. Continuous lines are Boltzmann fits to the experimental data. Each data point is the mean ± SEM of 13–18 cells recorded in at least three separate experimental sessions. ***C***, Western blot analysis of proteins from total lysates (top) or streptavidin-purified biotinylated plasma membrane fractions (bottom) from nontransfected CHO cells (NT) or from CHO cells transfected with $K_v7.3$, $K_v7.3$ A315T, or $K_v7.3$ R230C plasmids. In each panel, the higher and lower blots were probed with anti-$K_v7.3$ or anti-α-tubulin antibodies, as indicated. NT (t.l.) and $K_v7.3$ (t.l.) indicate the lanes corresponding to total lysates from nontransfected or $K_v7.3$-expressing cells, loaded on the gel-containing biotinylated proteins to visualize the molecular mass of $K_v7.3$ and α-tubulin. Numbers on the left correspond to the molecular masses of the protein marker. Quantitative analysis of the data is given in the text.

Compared with homomeric $K_v7.2$, heteromeric $K_v7.2/3$ channels displayed a reduced TEA sensitivity, a slight leftward shift of activation gating, and a drastic increase in maximal current density (Wang et al., 1998). Incorporation of $K_v7.2$ R201C, $K_v7.2$ R201H, or $K_v7.3$ R230C mutant subunits into heteromers prompted changes in channel gating that were similar, although quantitatively less dramatic, than those described in homomeric channels carrying mutant subunits (Fig. 4; Table 1). The resting membrane potential was significantly more negative in cells expressing heteromeric channels carrying mutant subunits than wild-type $K_v7.2/3$ channels, a result consistent with the reported hyperpolarizing shift in activation gating; as expected, changes in resting membrane potential among groups disappeared when the cells were depolarized using a higher (50 mM) extracellular K^+ concentration (Table 1). Gating changes in triple heteromeric channels incorporating $K_v7.2$ R144Q subunits showed a similar, though statistically nonsignificant, trend (Table 1). In all cases, no changes in current size and TEA sensitivity were observed upon incorporation of mutant subunits, suggesting that these mutations failed to interfere with heteromeric subunit assembly (Table 1).

Homomeric $K_v7.2$ channels may contribute to I_{KM} diversity at some neuronal sites (Martire et al., 2004; Schwarz et al., 2006), particularly at early developmental stages (Devaux et al., 2004); therefore, the effects of each $K_v7.2$ mutation were also studied in heteromeric configuration with wild-type $K_v7.2$ subunits (1:1 ratio). Under this experimental condition, which generated a larger proportion of channels containing two mutant subunits, the gating changes observed were intermediate between homomeric (four mutant subunits) and triple heteromeric channels (one mutant subunit); the largest effect was observed when $K_v7.2$ R201C subunits were incorporated, whereas quantitatively smaller (but statistically significant) effects were observed upon incorporation of subunits carrying the R201H or R144Q mutations (Table 1). Similar results were also observed when mutant $K_v7.2$ subunits were coexpressed with $K_v7.3$, and when $K_v7.3$ R230C subunits were expressed with $K_v7.2$, suggesting that the observed gating changes were proportional to the number of mutant subunits incorporated into heteromeric channels (Table 1).

VSD electrostatic interactions identified by multistate structural analysis

As described, three of the four mutations herein investigated affect R2. To gain structural insights into the molecular mechanism by which this residue regulates gating in K_v7 channels, its electrostatic interactions were probed by multistate structural

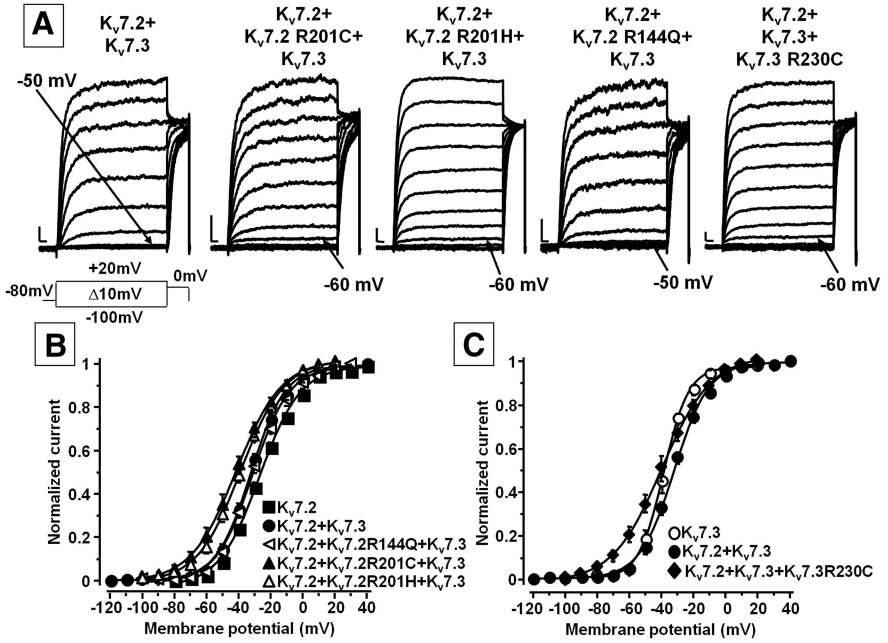

Figure 4. Functional properties of heteromeric channels incorporating subunits carrying EE mutations. ***A***, Macroscopic current traces from the indicated heteromeric channels in response to the indicated voltage protocol. Current scale, 200 pA; time scale, 0.1 s. Arrows indicate the threshold voltage (in mV) for current activation. Conductance/voltage curves for $K_v7.2$, $K_v7.2+K_v7.3$, $K_v7.2+K_v7.2$ R144Q$+K_v7.3$, $K_v7.2+K_v7.2$ R201C$+K_v7.3$, and $K_v7.2+K_v7.2$ R201H$+K_v7.3$ (***B***) or $K_v7.3$, $K_v7.2+K_v7.3$, and $K_v7.2+K_v7.3$ R230C$+K_v7.3$ (***C***). ***B***, ***C***, Continuous lines indicate Boltzmann fits of the experimental data. Current scale, 200 pA; time scale, 0.1 s. Each data point is the mean ± SEM of 6–12 cells recorded in at least three separate experimental sessions.

Table 2. Interactions between $K_v7.2$ R201 and negatively charged residues in the VSD of each $K_v7.2$ subunit

States	Subunit A	Subunit B	Subunit C	Subunit D
Activated	None	None	None	None
Early deactivated	None	E130	None	E130
Late deactivated	None	E130	None	E140
Resting	D172	None	E140	E140, D172
Early activated	E130	E140	None	D172
Late activated	None	None	None	None

modeling; by this technique, structural models of six VSD gating states (activated, early deactivated, late deactivated, resting, early activated, and late activated) can be built based on long (>200 μs) molecular dynamic simulations of the $K_v1.2/K_v2.1$ chimera (Long et al., 2007) subjected to depolarizing and hyperpolarizing voltages (Jensen et al., 2012). The primary sequences of the VSDs of $K_v7.2$ and $K_v7.3$ are very similar; thus, only data for $K_v7.2$ are shown, but similar conclusions can be drawn for $K_v7.3$. Given the asymmetric structural transitions occurring in the four VSDs, Table 2 lists the electrostatic interactions involving R2 in each $K_v7.2$ subunit at all six gating states, whereas the structural models of the six states of the D subunit only are shown in Figure 5. The results obtained suggest that R2 interacts differentially in each subunit with negatively charged residues E130 or E140 in S2, or D172 in S3 in the resting, early activated, late deactivated, or early deactivated state, whereas no interaction with these residues occurs when the VSD occupies the late activated and fully activated states. As expected (Long et al., 2007; Miceli et al., 2008, 2013), in the present model E130, E140, and D172, in addition to R2, also interact with other S4 positively charged residues in different gating states.

Probing the interactions involving the R201 residue in $K_v7.2$ by coupled charge reversal or disulfide trapping

To probe with functional experiments R2 interactions highlighted by multistate modeling, electrophysiological experiments were performed in cells expressing $K_v7.2$ channels where R2-interacting E130, E140, and D172 residues were substituted with positively charged (E130R, E140R, or D172R) or cysteine (E130C, E140C, or D172C) residues, alone or in combination with R201 charge reversal (E130R/R201E, E140R/R201E, and D172R/R201D), or cysteine introduction (E130C/R201C, E140C/R201C, and D172C/R201C); the occurrence of a specific interaction between mutated residues could be hypothesized when the functional properties of channels formed by these double-mutant subunits were different from those of either single mutant.

Homomeric $K_v7.2$ channels carrying R201D or R201E mutations, similarly to R201C, elicited time- and voltage-independent currents (for $K_v7.2$ R201D and $K_v7.2$ R201E, the current densities were 53.1 ± 5.6 pA/pF and 27.7 ± 4.4 pA/pF, and the $I_{Instant}/I_{steady\text{-}state}$ ratios 0.98 ± 0.01 and 0.76 ± 0.02, respectively; n = 5–27), again suggesting that the positive charge at R2 is a critical voltage-sensing element (Miceli et al., 2008). Compared with $K_v7.2$, current activation from homomeric $K_v7.2$ E130R and E130C mutant channels was rightwardly shifted (the $V_{½}$ were 59.5 ± 3.4 and 1.2 ± 0.2 mV, respectively; n = 7–8; $p < 0.05$ vs $K_v7.2$), whereas $K_v7.2$ E130R/R201E or $K_v7.2$ E130C/R201C double-mutant channels, similarly to $K_v7.2$ R201E and R201C, showed time- and voltage-independent gating (the $I_{Instant}/I_{steady\text{-}state}$ ratios were 0.93 ± 0.02 or 0.91 ± 0.02, respectively; n = 6–18); by contrast, all mutations involving the E140 residue (E140R, E140C, E140R/R201E, and E140C/R201C) were functionally silent (current densities at 0 mV were 0.8 ± 0.1, 0.2 ± 0.1, 0.6 ± 0.2, or 0.5 ± 0.1 pA/pF, respectively; n = 5–23; $p > 0.05$ vs untransfected CHO cells). Thus, no significant functional difference could be detected between E130/R2 or E140/R2 doubly mutated channels, and one of the single mutants.

Instead, homomeric $K_v7.2$ D172R or D172C single mutant channels were functional (for $K_v7.2$ D172R and Kv7.2 D172C, the current densities were 13.2 ± 2.2 pA/pF and 54.7 ± 13 pA/pF; n = 9–14), although their activation gating was rightwardly shifted (the $V_{½}$ were −11.9 ± 1.5 and −4 ± 1.3 mV for $K_v7.2$ D172R and $K_v7.2$ D172C, respectively; n = 9–14; $p < 0.05$ vs Kv7.2), whereas $K_v7.2$ D172R/R201D and D172C/R201C double-mutant channels were nonfunctional (current densities at 0 mV were 1.1 ± 0.2 and 0.3 ± 0.1 pA/pF, respectively; n = 8–20; $p > 0.05$ vs untransfected CHO cells), despite being expressed at the plasma membrane similarly to $K_v7.2$ subunits. Indeed, the $OD_{Q2\text{-}TOTAL}/OD_{TUB}$ ratios were 1.00 ± 0.14, 1.17 ± 0.11, and 0.84 ± 0.14 for $K_v7.2$, $K_v7.2$ D172R/R201D, and $K_v7.2$ D172C/R201C, respectively; and the $OD_{Q2\text{-}BIOT}/OD_{Q2\text{-}TOTAL}$ ratios were 1.06 ± 0.24, 0.94 ± 0.25, and 0.66 ± 0.09 for $K_v7.2$, $K_v7.2$ D172R/R201D, and $K_v7.2$ D172C/R201C, respectively (n = 3; $p > 0.05$) (Fig. 6*A*). The fact that D172R/R201D or

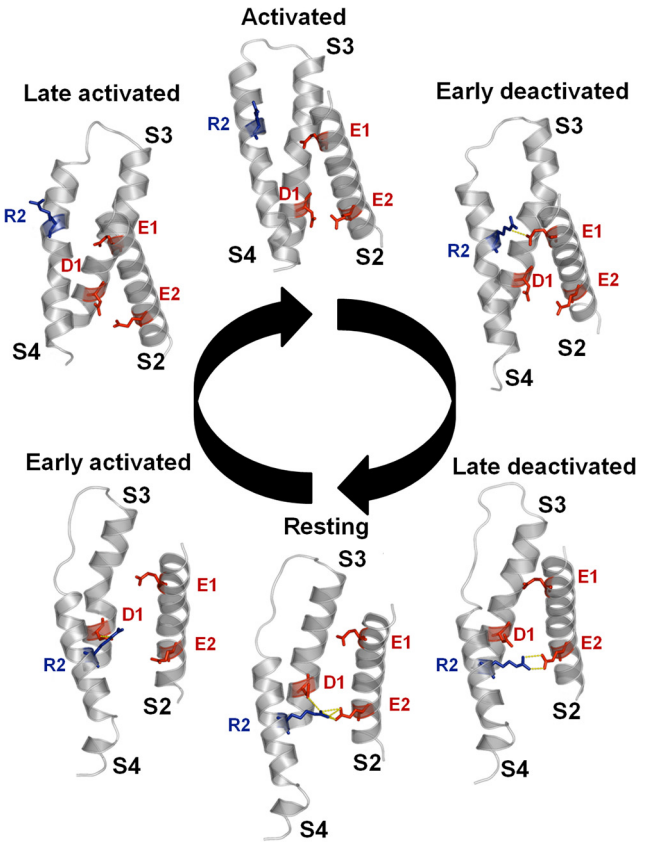

Figure 5. Structural modeling of $K_v7.2$ VSD in six gating states. The structural model of six gating states (activated, early deactivated, late deactivated, resting, early activated, and late activated) of $K_v7.2$ VSD is shown. Red represents negatively charged E130 (E1), E140 (E2), and D172 (D1) residues. Blue represents positively charged R201 (R2) residue. Yellow represents electrostatic interactions. For clarity, only the S2, S3, and S4 transmembrane segments, and the S3–S4 interconnecting loop, are shown.

$K_v7.2$ D172C/R201C subunits are present in the plasma membrane fraction but are unable to form functional channels, whereas D172R, D172C, R201D, or R201C channels all carry large currents, is suggestive of a possible VSD resting state hyperstabilization caused by a newly formed intrasubunit interaction.

To challenge this hypothesis, we studied the effects of the strong reducing agent and disulfide bond breaker dithiothreitol (DTT) in $K_v7.2$ D172C/R201C channels. Treatment for 1 h of cells expressing nonfunctional $K_v7.2$ D172C/R201C double-mutant channels with DTT (1 mM) elicited a small but detectable current upon depolarization to 0 mV (Fig. 6*B*); this current was almost fully (85.4 ± 3.4% of inhibition; $n = 3$) and reversibly blocked by 3 mM TEA (Fig. 6*B*). The effect of DTT was highly specific for the double mutant, as either $K_v7.2$, $K_v7.2$ D172C or R201C single mutant channels were insensitive to DTT (Fig. 6*C*). H_2O_2 (500 μM) fully reversed DTT-induced current increase in $K_v7.2$ D172C/R201C channels. These data provide functional evidence for the occurrence of a disulfide bond when cysteines occupy both the 172 and 201 positions, suggesting that electrostatic interactions between these residues are likely to occur in native $K_v7.2$ channels. By contrast, treatment with retigabine (10 μM), despite promoting channel opening allosterically, failed to recover currents from Kv7.2 D172R/R201D channels; indeed, the current density at 0 mV was 0.5 + 0.2 pA/pF before drug exposure (control) and 0.5 + 0.2 pA/pF upon retigabine exposure ($n = 5$ cells; $p > 0.05$).

Network interactions may explain the increase of CA1 excitability caused by I_{KM} GOF mutation

To test the possible mechanisms underlying the $K_v7.2/3$ mutation-induced increase in excitability, we first tested intrinsic cell properties using a realistic model of a hippocampal principal neuron. An increase in a K^+ current, such as I_{KM}, results in a hyperpolarization of the resting membrane potential, which may increase the availability of Na^+ channels. In our CA1 model cell, the hyperpolarization induced by I_{KM} was 0.21 and 0.63 mV for wild-type ($K_v7.2$+Kv7.3) and mutant ($K_v7.2$+$K_v7.2$ R201C+$K_v7.3$) I_{KM}, respectively. This effect may be particularly important for CA1 during a train of action potentials because, in these cells, dendritic Na^+ channels exhibit slow inactivation with a strong voltage dependence (Spruston et al., 1995). In principle, thus, the larger hyperpolarization generated by a mutant I_{KM} can increase cell's excitability. This effect is illustrated by the simulations in Fig. 7*A*. Under control conditions (Fig. 7*A*, blue trace, wild-type I_{KM}), a few spikes were elicited at the beginning of the simulation; as soon as the dendritic Na^+ channels inactivate (after ~100 ms) the cell stops firing. However, a hyperpolarizing current (Fig. 7*A*, red trace, −4 nA) rescued Na^+ channels from the inactivated state, and a few more spikes were elicited at the end of the current injection. Because the mutant I_{KM} hyperpolarized the somatic resting potential by only 0.43 mV, additional Na^+ channel repriming was marginal (Fig. 7*A*, black trace), and increasing the I_{KM} peak conductance resulted in qualitatively similar effects (data not shown). The model thus suggests that an increased availability of Na^+ channels does not appear to be responsible for an increased excitability of hippocampal CA1 pyramidal cells.

We next tested a feedforward inhibitory microcircuit, implemented as shown in Fig. 7*B* (left). The rationale for this choice is that the intrinsic properties of different cells can be differentially affected by the same $K_v7.2/3$-I_{KM} mutation. To test this hypothesis, we explored different combinations for the average excitatory input frequency and the peak excitatory conductance activating the interneuron, whereas the peak inhibitory conductance on the CA1 was fixed at 150 nS, corresponding to the synchronous activation of ~30–100 inhibitory synapses (Bertrand and Lacaille, 2001). For the combination of parameters indicated in Figure 7*B* (right, star), incorporating of the experimentally defined parameters for mutant I_{KM} resulted in a 190% increase in the number of action potentials elicited in the pyramidal neuron. This difference depends on the interneuron activity. A weaker activation will result in a smaller difference between wild-type and mutant I_{KM} (Fig. 7*B*, green area in the plot), whereas a stronger interneuron activation will make the effect of the mutation less important and the CA1 will appear less excitable (Fig. 7*B*, orange areas in the plot). As shown in Figure 7*C*, under control conditions (blue and red traces), the interneuron activity blocks more than half of the action potentials that would be generated by the excitatory input on CA1. However, in the presence of a mutated I_{KM} (green and black traces), the resting potential of the interneuron will be much more hyperpolarized with respect to that with wild-type I_{KM} (8.63 vs 3.16 mV, compare green and black membrane potential at the beginning of the simulation in Fig. 7*C*), an effect directly related to the higher input resistance of the interneuron. This larger hyperpolarization limits the interneuron activation and results in an effective disinhibition of the principal cell, which now appears as more excitable. Because in hippocampal interneurons I_{KM} appears to be also expressed in dendrites (Lawrence et al., 2006), we also tested a uniform somatodendritic expression of I_{KM} in the dendrites of the interneuron. The results (data not shown) were qualitatively similar to those obtained

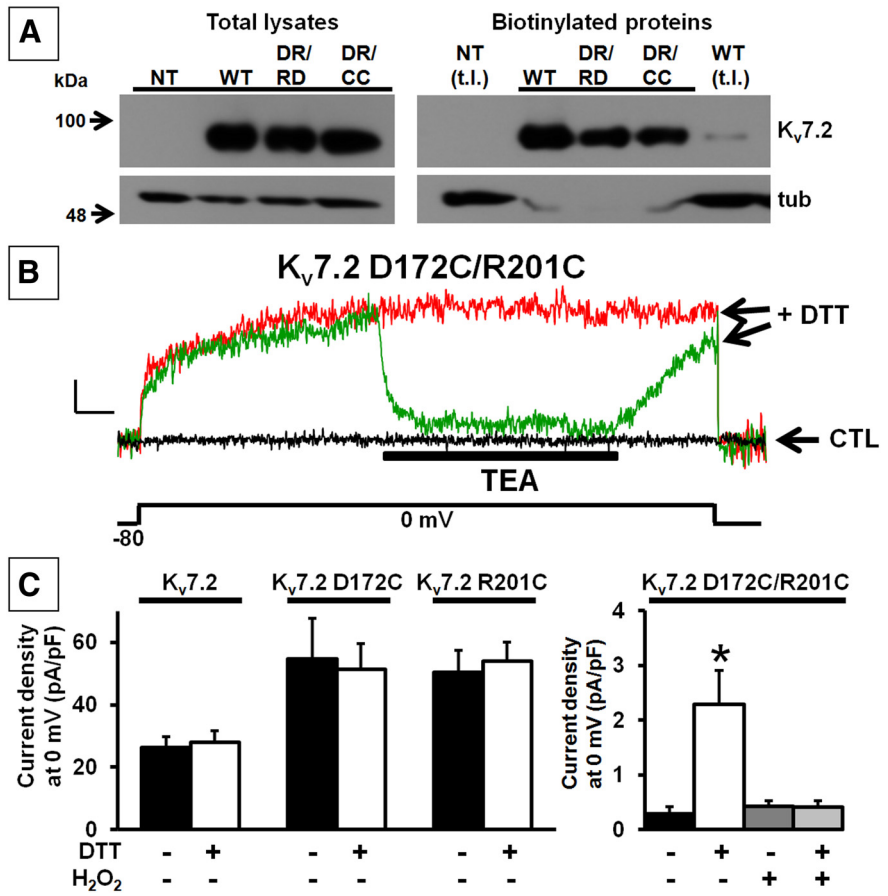

Figure 6. Membrane expression of $K_v7.2$ D172R/R201D and D172C/R201C channels, and effects of reducing/oxidizing agents on $K_v7.2$ cysteine-substituted channels. ***A***, Western blot analysis of proteins from total lysates (left) or streptavidin-purified biotinylated plasma membrane fractions (right) from untransfected CHO cells (NT) or from CHO cells expressing $K_v7.2$ (WT), $K_v7.2$ D172R/R201D (DR/RD), or D172C/R201C (DR/CC) subunits. In each panel, the higher and lower blots were probed with anti-$K_v7.2$ or anti-α-tubulin antibodies, as indicated. NT (t.l.) and WT (t.l.) indicate the lanes corresponding to total lysates from nontransfected (NT) or $K_v7.2$-expressing (WT) cells, loaded on the gel containing biotinylated proteins to visualize the molecular mass of $K_v7.2$ and α-tubulin. Numbers on the left correspond to the molecular masses of the protein marker. Quantitative analysis of the data is given in the text. ***B***, Superimposed traces of current responses evoked by a 0 mV pulse from a CHO cell transfected with the plasmid encoding for $K_v7.2$ D172C/R201C subunits in control condition (CTL; black trace) or from another cell of the same experimental group after treatment with DTT (1 mM, red trace). Green trace represents the current response from the same DTT-treated $K_v7.2$ D172C/R201C-expressing cell shown in red during exposure to TEA (3 mM) and subsequent washout. Bar at bottom represents the duration of TEA exposure. Current scale, 20 pA; time scale, 0.5 s. ***C***, Quantification of current densities and effect of DTT (1 mM), H_2O_2 (0.5 mM), and DTT + H_2O_2 from the indicated channels. $*p < 0.05$, significantly different from the respective control. $N = 4–10$ cells per group recorded in at least three separate experimental sessions.

with the somatic only expression, and implicitly confirm the robustness of the observed effect. Together, these results suggest that a GOF mutation in $K_v7.2/3$-I_{KM} can increase the (apparent) excitability of hippocampal CA1 pyramidal neurons by altering network interactions rather than the intrinsic cell properties.

Discussion

$K_v7.2$ and $K_v7.3$ VSD mutations associated with EEs promote GOF effects on channel gating

$K_v7.2$ and, to a lesser degree, $K_v7.3$ mutations have been associated with a wide phenotypic spectrum of epileptic disorders, ranging from BFNS to early-onset EEs. In the present work, we studied the functional consequences of three $K_v7.2$ and one $K_v7.3$ *de novo* mutations found by classical Sanger sequencing (R201C in $K_v7.2$; Weckhuysen et al., 2013), targeted gene resequencing (R201H in $K_v7.2$; Carvill et al., 2013), or whole-exome sequencing (R144Q in $K_v7.2$ and R230C in $K_v7.3$; Allen et al., 2013) in individuals affected with various forms of EEs; notably, a child with nonsyndromic intellectual disability and multifocal epileptic activity also carried the R230C variant in $K_v7.3$ (Rauch et al., 2012), confirming the tight genetic interconnection between EEs and intellectual disability and/or autism spectrum disorders (Novarino et al., 2013). Notably, the R144Q mutation occurs in a patient who did not suffer from neonatal seizures but rather showed infantile spasms with a later (6 months) age of onset (Allen et al., 2013).

Both in homomeric or heteromeric configuration with $K_v7.2/3$ subunits, the mutations herein investigated increased channel sensitivity to voltage, without major changes in pore properties, heteromerization, and/or membrane expression. Indeed, current activation midpoint in homomeric $K_v7.2$ R144Q channels, which neutralized a highly conserved R at the bottom of S2, was hyperpolarized by ~20 mV. By contrast, homomeric channels formed by $K_v7.2$ R201C or $K_v7.3$ R230C subunits, in which the crucial gating residue R2 was replaced by a mostly neutral C, displayed a marked loss in voltage-dependent gating. The fact that the gating changes of $K_v7.2$ R201H channels were quantitatively smaller than those of R201C channels is consistent with the notion that the removal of the positive charge is in itself responsible for the observed gating alterations; indeed, under physiological pH, histidines are mostly uncharged (pKa is ~6), but a small percentage could be protonated, whereas cysteines, having a pKa of ~8.4, are partly (10%) deprotonated and negatively charged. In keeping with this hypothesis, R201D and R201E, similarly to R201Q $K_v7.2$ channels (Miceli et al., 2008), also carried time- and voltage-independent currents. Neutralization of the corresponding position in $K_v7.1$ (Panaghie and Abbott, 2007) or $K_v7.4$ (Miceli et al., 2012) led to similar gating changes. Single-channel measurements in $K_v7.2$ R201Q channels (Miceli et al., 2008) showed that this mutation affected the conformational changes involving deeper, nonconducting closed states, where most of the voltage-dependent transitions occur (Zagotta and Aldrich, 1990).

Structural insight into R2 involvement in K_v7 channel gating

Multistate molecular modeling revealed that R2 forms ionized hydrogen bonds with different negatively charged residues (E130 and E140 in S2, D172 in S3) in distinct states along the activation/deactivation trajectories of each subunit. No ionized hydrogen bond involving R2 can be detected in the fully activated and late activated states, whereas significant electrostatic interactions occur in the resting and nearby states. Thus, mutations substituting R2 with mostly uncharged H or C residues would preferentially weaken the stability of the resting, fully deactivated state of the

VSD, without significantly compromising that of the activated state; consistent with our functional data, this stability shift toward the activated state would allow the channels to be more easily opened by voltage, with a significant fraction being already active at hyperpolarized membrane potentials. Disulfide trapping experiments showed that $K_v7.2$ D172C/R201C channels were rescued from nonfunctional to active upon DTT reduction, an effect reverted by H_2O_2 and requiring the simultaneous presence of C residues at both these positions. Given that side chains thiols can form a disulfide bond when the distance between their Cβ atoms reaches ~4.6 Å (although this value is critically dependent on protein flexibility) (Careaga and Falke, 1992), these data provide functional evidence for the occurrence of an ionized hydrogen bond between D172 and R201 stabilizing the resting state of the VSD in $K_v7.2$.

Potential mechanism(s) for neuronal dysfunction by $K_v7.2/3$ GOF mutations

Mutations in $K_v7.2/3$ responsible for both familial and sporadic cases of BFNS decrease channel function by several mechanisms, including gating defects (Dedek et al., 2001; Castaldo et al., 2002; Soldovieri et al., 2007), decreased subunit stability (Soldovieri et al., 2006), altered subcellular targeting (Chung et al., 2006; Liu and Devaux, 2014), or defective regulation by calmodulin (Cavaretta et al., 2014) or syntaxin-1A (Soldovieri et al., 2014). The main conclusion from the present study is that, in addition to dramatic functional deficits (Miceli et al., 2013), in some cases with dominant-negative consequences (Orhan et al., 2014), *de novo* mutations found in EE patients can also enhance $K_v7.2/3$ channel function.

Epilepsy-causing GOF mutations in K^+ channel genes have been reported previously, as in the case of *KCNMA1* encoding for the α-subunit of large conductance calcium-sensitive (BK) channels (Du et al., 2005), of *KCNJ10* encoding for the inwardly rectifying $K_{IR}4.1$ channel (Sicca et al., 2011), and of *KCND2* encoding for the A-type channel $K_v4.2$ (Lee et al., 2014). Moreover, an increased voltage sensitivity favoring channel opening is caused by the $K_v10.2$ (*KCNH5*) R327H mutation (also affecting the VSD R2 residue) (Yang et al., 2013) found in children with EE and autistic features (Veeramah et al., 2013), and constitutive channel activation characterizes KCNT1 mutations occurring in malignant migrating partial seizures of infancy (Barcia et al., 2012); in KCNT1 mutants, treatment with quinidine restored normal channel function, highlighting novel therapeutic strategies for malignant migrating partial seizures of infancy (Milligan et al., 2014).

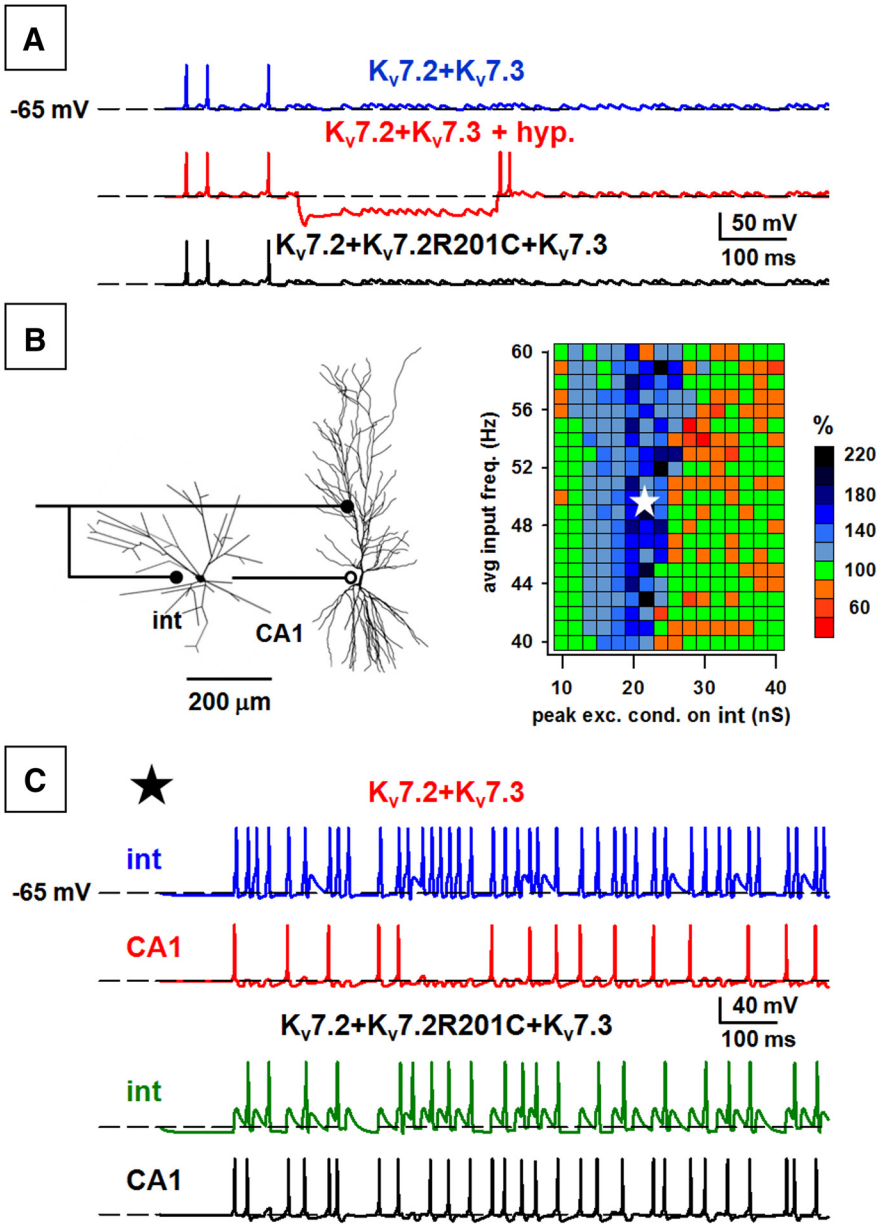

Figure 7. A computational model suggests the possible physiological mechanism for the increase in CA1 excitability following a GOF mutation of I_{KM}. ***A***, Increased Na^+ channel availability may not account for the increase in excitability; traces are from simulations under control conditions, using wild-type I_{KM} ($K_v7.2+Kv7.3$, blue), control conditions with a −4 nA hyperpolarizing current injection (red), and with mutant I_{KM} channels ($K_v7.2+K_v7.2$ R201C$+K_v7.3$, black). Dashed line indicates the resting potential, set at −65 mV; the same synaptic stimulation pattern was used for all cases. ***B***, Left, The microcircuit used to test the effects of a mutant I_{KM}: an input activates excitatory synapses (closed circles) on the CA1 pyramidal neuron and, with a 3 ms delay, on the interneuron; somatic spikes of the interneuron activate an inhibitory synapse (open circle) on the soma of the CA1 cell. Right, Relative change in the number of CA1 action potentials elicited as a function of the average input frequency and the peak excitatory conductance on the interneuron. ★Case shown in detail in ***C***. ***C***, Somatic membrane potential for the two cells in the simulations indicated in ***B*** (☆). There is large hyperpolarization of the interneuron caused by the mutant I_{KM} (green).

Several pathophysiological mechanisms have been proposed to explain the apparently paradoxical increase in brain excitability caused by GOF mutations in K^+ channels; although $K_{IR}4.1$ mutations may trigger a recurrent neuron-astrocyte-neuron excitatory loop (Sicca et al., 2011), hyperactivation of BK channels would enable higher firing frequencies in excitatory neurons because of faster action potential repolarization and sodium channel repriming (Du et al., 2005). Alternatively, an increased function of subthreshold K^+ channels, such as I_{KM} (Hu et al., 2009; Nigro et al., 2014), may overactivate the hyperpolarization-

activated nonselective cation current I_h (Robinson and Siegelbaum, 2003), resulting in secondary depolarizations. The present computational modeling experiments suggest that an increased function of I_{KM} is unable to increase principal neuron excitability by Na^+ channels repriming because the increase in the Na^+ channels availability is not sufficient to counterbalance the mutation-induced hyperpolarization; instead, because of the larger input resistance observed in interneurons compared with principal neurons (Foster and Dumas, 2001; Lamsa et al., 2007; Zemankovics et al., 2010), a negative shift in I_{KM} would preferentially affect the inhibitory interneuron, thereby leading to an increased excitability of the principal neuron. Although compensatory homeostatic mechanisms, such as the relocation of the axon initial segment (Harty et al., 2013) should also be taken into account, an impairment in the delicate balance between excitation and inhibition in hippocampal CA1 pyramidal neurons seems to contribute to the epileptic phenotype. Therefore, K_v7 GOF mutations can affect hippocampal theta oscillation involved in cognitive processes, such as learning and memory, which depends on I_{KM} function through the so-called somatic M-resonance (Hu et al., 2009). Noteworthy, selective silencing of inhibitory interneurons also occurs in epileptic channelopathies caused by SCN1A LOF mutations (Catterall et al., 2010).

The present results reveal that complex network properties, rather than intrinsic properties of isolated principal neurons (Miceli et al., 2013), contribute to cellular hyperexcitability by I_{KM} GOF mutations, suggesting that reducing or enhancing I_{KM} may trigger epileptogenesis by different pathophysiological mechanisms. Similarly, although most *de novo* mutations in the I_h-encoding *HCN1* gene occurring in patients with infantile EE cause GOF effects, few promoted LOF, and both decreases or increases in I_h have been suggested as pathogenic *in vivo* (Nava et al., 2014).

K_v7 channels may serve contrasting functional roles depending on their subcellular localization (Kole and Cooper, 2014). Indeed, whereas perisomatic Kv7 channels counteract the persistent Na_v current and restrain repetitive firing, K_v7 channels in nodes of Ranvier of neocortical (Battefeld et al., 2014) and hippocampal (Vervaeke et al., 2006) neurons, in addition to preventing aberrant spontaneous firing, can also increase Na_v channel availability and action potential amplitude by hyperpolarizing the resting membrane potential and removing Na_v inactivation; thus, $K_v7.2/3$ mutations may differentially affect neuronal excitability in a context-dependent manner because of differences in intrinsic biophysical properties or modulation by regulatory partners at each subcellular site.

The present results do not cover the full spectrum of possible mechanisms of mutation-induced channel dysfunction; thus, caution should be exercised if these are used to formulate hypotheses on disease pathogenesis. Indeed, the $K_{IR}3.2$ mutation responsible for the *weaver* phenotype in mice promoted GOF effects when channels were expressed heterologously but impaired channel trafficking and function *in vivo* (Kofuji et al., 1996; Rossi et al., 1998). Nonetheless, because highly sensitive genome sequencing techniques are likely to be introduced in routine clinical practice in the near future, the interpretation of the pathogenic role of specific gene variants and genotype-phenotype correlations will have a significant impact not only on disease diagnosis, but also for patient-tailored prognostic and therapeutic approaches. The present description of $K_v7.2/3$ GOF mutations associated with EEs reveals a previously unexplored level of complexity in disease pathogenesis, which requires special attention when investigating the effect of K_v7 modulators on cognitive and other neurodevelopmental outcomes (Weckhuysen et al., 2012; Miceli et al., 2013; Orhan et al., 2014).

References

Allen AS, Berkovic SF, Cossette P, Delanty N, Dlugos D, Eichler EE, Epstein MP, Glauser T, Goldstein DB, Han Y, Heinzen EL, Hitomi Y, Howell KB, Johnson MR, Kuzniecky R, Lowenstein DH, Lu YF, Madou MR, Marson AG, Mefford HC, et al. (2013) De novo mutations in epileptic encephalopathies. Nature 501:217–221. CrossRef Medline

Ascoli GA, Gasparini S, Medinilla V, Migliore M (2010) Local control of postinhibitory rebound spiking in CA1 pyramidal neuron dendrites. J Neurosci 30:6434–6442. CrossRef Medline

Barcia G, Fleming MR, Deligniere A, Gazula VR, Brown MR, Langouet M, Chen H, Kronengold J, Abhyankar A, Cilio R, Nitschke P, Kaminska A, Boddaert N, Casanova JL, Desguerre I, Munnich A, Dulac O, Kaczmarek LK, Colleaux L, Nabbout R (2012) De novo gain-of-function KCNT1 channel mutations cause malignant migrating partial seizures of infancy. Nat Genet 44:1255–1259. CrossRef Medline

Battefeld A, Tran BT, Gavrilis J, Cooper EC, Kole MH (2014) Heteromeric Kv7.2/7.3 channels differentially regulate action potential initiation and conduction in neocortical myelinated axons. J Neurosci 34:3719–3732. CrossRef Medline

Bertrand S, Lacaille JC (2001) Unitary synaptic currents between lacunosum-moleculare interneurones and pyramidal cells in rat hippocampus. J Physiol 532:369–384. CrossRef Medline

Biervert C, Schroeder BC, Kubisch C, Berkovic SF, Propping P, Jentsch TJ, Steinlein OK (1998) A potassium channel mutation in neonatal human epilepsy. Science 279:403–406. CrossRef Medline

Borgatti R, Zucca C, Cavallini A, Ferrario M, Panzeri C, Castaldo P, Soldovieri MV, Baschirotto C, Bresolin N, Dalla Bernardina B, Taglialatela M, Bassi MT (2004) A novel mutation in KCNQ2 associated with BFNC, drug resistant epilepsy, and mental retardation. Neurology 63:57–65. CrossRef Medline

Careaga CL, Falke JJ (1992) Thermal motions of surface alpha-helices in the D-galactose chemosensory receptor: detection by disulfide trapping. J Mol Biol 226:1219–1235. CrossRef Medline

Carvill GL, Heavin SB, Yendle SC, McMahon JM, O'Roak BJ, Cook J, Khan A, Dorschner MO, Weaver M, Calvert S, Malone S, Wallace G, Stanley T, Bye AM, Bleasel A, Howell KB, Kivity S, Mackay MT, Rodriguez-Casero V, Webster R, et al. (2013) Targeted resequencing in epileptic encephalopathies identifies de novo mutations in CHD2 and SYNGAP1. Nat Genet 45:825–830. CrossRef Medline

Castaldo P, del Giudice EM, Coppola G, Pascotto A, Annunziato L, Taglialatela M (2002) Benign familial neonatal convulsions caused by altered gating of KCNQ2/KCNQ3 potassium channels. J Neurosci 22:RC199. Medline

Castaldo P, Stefanoni P, Miceli F, Coppola G, Del Giudice EM, Bellini G, Pascotto A, Trudell JR, Harrison NL, Annunziato L, Taglialatela M (2004) A novel hyperekplexia-causing mutation in the pre-transmembrane segment 1 of the human glycine receptor alpha1 subunit reduces membrane expression and impairs gating by agonists. J Biol Chem 279:25598–25604. CrossRef Medline

Catterall WA, Kalume F, Oakley JC (2010) NaV1.1 channels and epilepsy. J Physiol 588:1849–1859. CrossRef Medline

Cavaretta JP, Sherer KR, Lee KY, Kim EH, Issema RS, Chung HJ (2014) Polarized axonal surface expression of neuronal KCNQ potassium channels is regulated by calmodulin interaction with KCNQ2 subunit. PLoS One 9:e103655. CrossRef Medline

Charlier C, Singh NA, Ryan SG, Lewis TB, Reus BE, Leach RJ, Leppert M (1998) A pore mutation in a novel KQT-like potassium channel gene in an idiopathic epilepsy family. Nat Genet 18:53–55. CrossRef Medline

Chung HJ, Jan YN, Jan LY (2006) Polarized axonal surface expression of neuronal KCNQ channels is mediated by multiple signals in the KCNQ2 and KCNQ3 C-terminal domains. Proc Natl Acad Sci U S A 103:8870–8875. CrossRef Medline

Cross JH, Guerrini R (2013) The epileptic encephalopathies. Handb Clin Neurol 111:619–626. CrossRef Medline

Dedek K, Kunath B, Kananura C, Reuner U, Jentsch TJ, Steinlein OK (2001) Myokymia and neonatal epilepsy caused by a mutation in the voltage sensor of the KCNQ2 K+ channel. Proc Natl Acad Sci U S A 98:12272–12277. CrossRef Medline

Devaux JJ, Kleopa KA, Cooper EC, Scherer SS (2004) KCNQ2 is a nodal K^+ channel. J Neurosci 24:1236–1244. CrossRef Medline

Du W, Bautista JF, Yang H, Diez-Sampedro A, You SA, Wang L, Kotagal P, Lüders HO, Shi J, Cui J, Richerson GB, Wang QK (2005) Calcium-sensitive potassium channelopathy in human epilepsy and paroxysmal movement disorder. Nat Genet 37:733–738. CrossRef Medline

Foster TC, Dumas TC (2001) Mechanism for increased hippocampal synaptic strength following differential experience. J Neurophysiol 85:1377–1383. Medline

Harty RC, Kim TH, Thomas EA, Cardamone L, Jones NC, Petrou S, Wimmer VC (2013) Axon initial segment structural plasticity in animal models of genetic and acquired epilepsy. Epilepsy Res 105:272–279. CrossRef Medline

Hines ML, Carnevale NT (1997) The NEURON simulation environment. Neural Comput 9:1179–1209. CrossRef Medline

Hu H, Vervaeke K, Storm JF (2002) Two forms of electrical resonance at theta frequencies, generated by M-current, h-current and persistent Na current in rat hippocampal pyramidal cells. J Physiol 545:783–805. CrossRef Medline

Hu H, Vervaeke K, Storm JF (2007) M-channels (Kv7/KCNQ channels) that regulate synaptic integration, excitability, and spike pattern of CA1 pyramidal cells are located in the perisomatic region. J Neurosci 27:1853–1867. CrossRef Medline

Hu H, Vervaeke K, Graham LJ, Storm JF (2009) Complementary theta resonance filtering by two spatially segregated mechanisms in CA1 hippocampal pyramidal neurons. J Neurosci 29:14472–14483. CrossRef Medline

Jensen MØ, Jogini V, Borhani DW, Leffler AE, Dror RO, Shaw DE (2012) Mechanism of voltage gating in potassium channels. Science 336:229–233. CrossRef Medline

Jentsch TJ (2000) Neuronal KCNQ potassium channels: physiology and role in disease. Nat Rev Neurosci 1:21–30. CrossRef Medline

Kato M, Yamagata T, Kubota M, Arai H, Yamashita S, Nakagawa T, Fujii T, Sugai K, Imai K, Uster T, Chitayat D, Weiss S, Kashii H, Kusano R, Matsumoto A, Nakamura K, Oyazato Y, Maeno M, Nishiyama K, Kodera H, et al. (2013) Clinical spectrum of early onset epileptic encephalopathies caused by KCNQ2 mutation. Epilepsia 54:1282–1287. CrossRef Medline

Kofuji P, Hofer M, Millen KJ, Millonig JH, Davidson N, Lester HA, Hatten ME (1996) Functional analysis of the weaver mutant GIRK2 K^+ channel and rescue of weaver granule cells. Neuron 16:941–952. CrossRef Medline

Kole MH, Cooper EC (2014) Axonal Kv7.2/7.3 channels: caught in the act. Channels 8:288–289. CrossRef Medline

Lamsa K, Irvine EE, Giese KP, Kullmann DM (2007) NMDA receptor-dependent long-term potentiation in mouse hippocampal interneurons shows a unique dependence on Ca^{2+}/calmodulin-dependent kinases. J Physiol 584:885–894. CrossRef Medline

Lawrence JJ, Saraga F, Churchill JF, Statland JM, Travis KE, Skinner FK, McBain CJ (2006) Somatodendritic Kv7/KCNQ/M channels control interspike interval in hippocampal interneurons. J Neurosci 26:12325–12338. CrossRef Medline

Lee H, Lin MC, Kornblum HI, Papazian DM, Nelson SF (2014) Exome sequencing identifies de novo gain of function missense mutation in KCND2 in identical twins with autism and seizures that slows potassium channel inactivation. Hum Mol Genet 23:3481–3489. CrossRef Medline

Liu W, Devaux JJ (2014) Calmodulin orchestrates the heteromeric assembly and the trafficking of KCNQ2/3 (Kv7.2/3) channels in neurons. Mol Cell Neurosci 58:40–52. CrossRef Medline

Long SB, Tao X, Campbell EB, MacKinnon R (2007) Atomic structure of a voltage-dependent K^+ channel in a lipid membrane-like environment. Nature 450:376–382. CrossRef Medline

Marcelin B, Chauvière L, Becker A, Migliore M, Esclapez M, Bernard C (2009) H channel-dependent deficit of theta oscillation resonance and phase shift in temporal lobe epilepsy. Neurobiol Dis 33:436–447. CrossRef Medline

Martire M, Castaldo P, D'Amico M, Preziosi P, Annunziato L, Taglialatela M (2004) M channels containing KCNQ2 subunits modulate norepinephrine, aspartate, and GABA release from hippocampal nerve terminals. J Neurosci 24:592–597. CrossRef Medline

Miceli F, Soldovieri MV, Hernandez CC, Shapiro MS, Annunziato L, Taglialatela M (2008) Gating consequences of charge neutralization of arginine residues in the S4 segment of K(v)7.2, an epilepsy-linked K^+ channel subunit. Biophys J 95:2254–2264. CrossRef Medline

Miceli F, Vargas E, Bezanilla F, Taglialatela M (2012) Gating currents from Kv7 channels carrying neuronal hyperexcitability mutations in the voltage-sensing domain. Biophys J 102:1372–1382. CrossRef Medline

Miceli F, Soldovieri MV, Ambrosino P, Barrese V, Migliore M, Cilio MR, Taglialatela M (2013) Genotype-phenotype correlations in neonatal epilepsies caused by mutations in the voltage sensor of K(v)7.2 potassium channel subunits. Proc Natl Acad Sci U S A 110:4386–4391. CrossRef Medline

Migliore M (2003) On the integration of subthreshold inputs from perforant path and Schaffer collaterals in hippocampal CA1 pyramidal neurons. J Comput Neurosci 14:185–192. CrossRef Medline

Migliore M, Ferrante M, Ascoli GA (2005) Signal propagation in oblique dendrites of CA1 pyramidal cells. J Neurophysiol 94:4145–4155. CrossRef Medline

Milligan CJ, Li M, Gazina EV, Heron SE, Nair U, Trager C, Reid CA, Venkat A, Younkin DP, Dlugos DJ, Petrovski S, Goldstein DB, Dibbens LM, Scheffer IE, Berkovic SF, Petrou S (2014) KCNT1 gain of function in 2 epilepsy phenotypes is reversed by quinidine. Ann Neurol 75:581–590. CrossRef Medline

Minneci F, Janahmadi M, Migliore M, Dragicevic N, Avossa D, Cherubini E (2007) Signaling properties of stratum oriens interneurons in the hippocampus of transgenic mice expressing EGFP in a subset of somatostatin-containing cells. Hippocampus 17:538–553. CrossRef Medline

Nava C, Dalle C, Rastetter A, Striano P, de Kovel CG, Nabbout R, Cancès C, Ville D, Brilstra EH, Gobbi G, Raffo E, Bouteiller D, Marie Y, Trouillard O, Robbiano A, Keren B, Agher D, Roze E, Lesage S, Nicolas A, et al. (2014) De novo mutations in HCN1 cause early infantile epileptic encephalopathy. Nat Genet 46:640–645. CrossRef Medline

Nigro MJ, Mateos-Aparicio P, Storm JF (2014) Expression and functional roles of Kv7/KCNQ/M-channels in rat medial entorhinal cortex layer II stellate cells. J Neurosci 34:6807–6812. CrossRef Medline

Novarino G, Baek ST, Gleeson JG (2013) The sacred disease: the puzzling genetics of epileptic disorders. Neuron 80:9–11. CrossRef Medline

Orhan G, Bock M, Schepers D, Ilina EI, Reichel SN, Löffler H, Jezutkovic N, Weckhuysen S, Mandelstam S, Suls A, Danker T, Guenther E, Scheffer IE, De Jonghe P, Lerche H, Maljevic S (2014) Dominant-negative effects of KCNQ2 mutations are associated with epileptic encephalopathy. Ann Neurol 75:382–394. CrossRef Medline

Panaghie G, Abbott GW (2007) The role of S4 charges in voltage-dependent and voltage-independent KCNQ1 potassium channel complexes. J Gen Physiol 129:121–133. CrossRef Medline

Rauch A, Wieczorek D, Graf E, Wieland T, Endele S, Schwarzmayr T, Albrecht B, Bartholdi D, Beygo J, Di Donato N, Dufke A, Cremer K, Hempel M, Horn D, Hoyer J, Joset P, Röpke A, Moog U, Riess A, Thiel CT, et al. (2012) Range of genetic mutations associated with severe non-syndromic sporadic intellectual disability: an exome sequencing study. Lancet 380:1674–1682. CrossRef Medline

Robinson RB, Siegelbaum SA (2003) Hyperpolarization-activated cation currents: from molecules to physiological function. Annu Rev Physiol 65:453–480. CrossRef Medline

Rossi P, De Filippi G, Armano S, Taglietti V, D'Angelo E (1998) The weaver mutation causes a loss of inward rectifier current regulation in premigratory granule cells of the mouse cerebellum. J Neurosci 18:3537–3547. Medline

Saitsu H, Kato M, Koide A, Goto T, Fujita T, Nishiyama K, Tsurusaki Y, Doi H, Miyake N, Hayasaka K, Matsumoto N (2012) Whole exome sequencing identifies KCNQ2 mutations in Ohtahara syndrome. Ann Neurol 72:298–300. CrossRef Medline

Schwarz JR, Glassmeier G, Cooper EC, Kao TC, Nodera H, Tabuena D, Kaji R, Bostock H (2006) KCNQ channels mediate IKs, a slow K^+ current regulating excitability in the rat node of Ranvier. J Physiol 573:17–34. CrossRef Medline

Shah MM, Migliore M, Valencia I, Cooper EC, Brown DA (2008) Functional significance of axonal Kv7 channels in hippocampal pyramidal neurons. Proc Natl Acad Sci U S A 105:7869–7874. CrossRef Medline

Sicca F, Imbrici P, D'Adamo MC, Moro F, Bonatti F, Brovedani P, Grottesi A, Guerrini R, Masi G, Santorelli FM, Pessia M (2011) Autism with seizures and intellectual disability: possible causative role of gain-of-function of the inwardly-rectifying K^+ channel Kir4.1. Neurobiol Dis 43:239–247. CrossRef Medline

Singh NA, Charlier C, Stauffer D, DuPont BR, Leach RJ, Melis R, Ronen GM, Bjerre I, Quattlebaum T, Murphy JV, McHarg ML, Gagnon D, Rosales TO, Peiffer A, Anderson VE, Leppert M (1998) A novel potassium chan-

nel gene, KCNQ2, is mutated in an inherited epilepsy of newborns. Nat Genet 18:25–29. CrossRef Medline

Singh NA, Otto JF, Dahle EJ, Pappas C, Leslie JD, Vilaythong A, Noebels JL, White HS, Wilcox KS, Leppert MF (2008) Mouse models of human KCNQ2 and KCNQ3 mutations for benign familial neonatal convulsions show seizures and neuronal plasticity without synaptic reorganization. J Physiol 586:3405–3423. CrossRef Medline

Soldovieri MV, Castaldo P, Iodice L, Miceli F, Barrese V, Bellini G, Miraglia del Giudice E, Pascotto A, Bonatti S, Annunziato L, Taglialatela M (2006) Decreased subunit stability as a novel mechanism for potassium current impairment by a KCNQ2 C terminus mutation causing benign familial neonatal convulsions. J Biol Chem 281:418–428. CrossRef Medline

Soldovieri MV, Cilio MR, Miceli F, Bellini G, Miraglia del Giudice E, Castaldo P, Hernandez CC, Shapiro MS, Pascotto A, Annunziato L, Taglialatela M (2007) Atypical gating of M-type potassium channels conferred by mutations in uncharged residues in the S4 region of KCNQ2 causing benign familial neonatal convulsions. J Neurosci 27:4919–4928. CrossRef Medline

Soldovieri MV, Boutry-Kryza N, Milh M, Doummar D, Heron B, Bourel E, Ambrosino P, Miceli F, De Maria M, Dorison N, Auvin S, Echenne B, Oertel J, Riquet A, Lambert L, Gerard M, Roubergue A, Calender A, Mignot C, Taglialatela M, et al. (2014) Novel KCNQ2 and KCNQ3 mutations in a large cohort of families with benign neonatal epilepsy: first evidence for an altered channel regulation by syntaxin-1A. Hum Mutat 35:356–367 CrossRef Medline

Spruston N, Schiller Y, Stuart G, Sakmann B (1995) Activity dependent action potential invasion and calcium influx into hippocampal CAl dendrites. Science 268:297–300. CrossRef Medline

Steinlein OK, Conrad C, Weidner B (2007) Benign familial neonatal convulsions: always benign? Epilepsy Res 73:245–249. CrossRef Medline

Striano P, de Jonghe P, Zara F (2013) Genetic epileptic encephalopathies: is all written into the DNA? Epilepsia 54 [Suppl 8]:22–26.

Veeramah KR, Johnstone L, Karafet TM, Wolf D, Sprissler R, Salogiannis J, Barth-Maron A, Greenberg ME, Stuhlmann T, Weinert S, Jentsch TJ, Pazzi M, Restifo LL, Talwar D, Erickson RP, Hammer MF (2013) Exome sequencing reveals new causal mutations in children with epileptic encephalopathies. Epilepsia 54:1270–1281. CrossRef Medline

Vervaeke K, Gu N, Agdestein C, Hu H, Storm JF (2006) Kv7/KCNQ/M-channels in rat glutamatergic hippocampal axons and their role in regulation of excitability and transmitter release. J Physiol 576:235–256. CrossRef Medline

Wang HS, Pan Z, Shi W, Brown BS, Wymore RS, Cohen IS, Dixon JE, McKinnon D (1998) KCNQ2 and KCNQ3 potassium channel subunits: molecular correlates of the M-channel. Science 282:1890–1893. CrossRef Medline

Weckhuysen S, Mandelstam S, Suls A, Audenaert D, Deconinck T, Claes LR, Deprez L, Smets K, Hristova D, Yordanova I, Jordanova A, Ceulemans B, Jansen A, Hasaerts D, Roelens F, Lagae L, Yendle S, Stanley T, Heron SE, Mulley JC, et al. (2012) KCNQ2 encephalopathy: emerging phenotype of a neonatal epileptic encephalopathy. Ann Neurol 71:15–25. CrossRef Medline

Weckhuysen S, Ivanovic V, Hendrickx R, Van Coster R, Hjalgrim H, Møller RS, Grønborg S, Schoonjans AS, Ceulemans B, Heavin SB, Eltze C, Horvath R, Casara G, Pisano T, Giordano L, Rostasy K, Haberlandt E, Albrecht B, Bevot A, Benkel I, et al. (2013) Extending the KCNQ2 encephalopathy spectrum: clinical and neuroimaging findings in 17 patients. Neurology 81:1697–1703. CrossRef Medline

Yang Y, Vasylyev DV, Dib-Hajj F, Veeramah KR, Hammer MF, Dib-Hajj SD, Waxman SG (2013) Multistate structural modeling and voltage-clamp analysis of epilepsy/autism mutation Kv10.2-R327H demonstrate the role of this residue in stabilizing the channel closed state. J Neurosci 33:16586–16593. CrossRef Medline

Zagotta WN, Aldrich RW (1990) Voltage-dependent gating of Shaker A-type potassium channels in *Drosophila* muscle. J Gen Physiol 95:29–60. CrossRef Medline

Zaika O, Hernandez CC, Bal M, Tolstykh GP, Shapiro MS (2008) Determinants within the turret and pore-loop domains of KCNQ3 K^+ channels governing functional activity. Biophys J 95:5121–5137. CrossRef Medline

Zemankovics R, Káli S, Paulsen O, Freund TF, Hájos N (2010) Differences in subthreshold resonance of hippocampal pyramidal cells and interneurons: the role of h-current and passive membrane characteristics. J Physiol 588:2109–2132. CrossRef Medline